

General relativistic study of astrophysical jets with internal shocks

Mukesh K. Vyas¹, Indranil Chattopadhyay¹ *

¹*Aryabhata Research Institute of Observational Sciences (ARIES), Manora Peak, Nainital-263002, India*

ABSTRACT

We explore the possibility of formation of steady internal shocks in jets around black holes. We consider a fluid described by a relativistic equation of state, flowing about the axis of symmetry ($\theta = 0$) in a Schwarzschild metric. We use two models for the jet geometry, (i) a conical geometry and (ii) a geometry with non-conical cross-section. Jet with conical geometry is smooth flow. While the jet with non-conical cross section undergoes multiple sonic point and even standing shock. The jet shock becomes stronger, as the shock location is situated further from the central black hole. Jets with very high energy and very low energy do not harbour shocks, but jets with intermediate energies do harbour shocks. One advantage of these shocks, as opposed to shocks mediated by external medium is that, these shocks have no effect on the jet terminal speed, but may act as possible sites for particle acceleration. Typically, a jet with energy $1.8 c^2$, will achieve a terminal speed of $v_\infty = 0.813c$ for jet with any geometry. But for a jet of non-conical cross-section for which the length scale of the inner torus of the accretion disc is $40r_g$, then in addition, a steady shock will form at $r_{\text{sh}} \sim 7.5r_g$ and compression ratio of $R \sim 2.7$. Moreover, electron-proton jet seems to harbour the strongest shock. We discuss possible consequences of such a scenario.

Key words: Black Holes, Jets and outflows, Hydrodynamics, Shock waves

* Email:mukesh.vyas@aries.res.in (MKV); indra@aries.res.in (IC)

1 INTRODUCTION

The denomination relativistic jets was first used in the extra-galactic context by Baade & Minkowski (1954), while observing knots in optical waveband in galaxy M87. However, it is after the advent of radio astronomy, that the relativistic jets have been recognized as a very common phenomenon in astrophysics and is associated with various kinds of astrophysical objects such as active galactic nuclei (AGN e.g., M87), gamma ray bursts (GRB), young stellar objects (YSO e.g., HH 30, HH 34), X-ray binaries (*e.g.*, SS433, Cyg X-3, GRS 1915+105, GRO 1655-40) etc. In this paper, we discuss about jets which are associated around X-ray binaries like GRS1915+105 (Mirabel & Rodriguez 1994) and AGNs like 3C273, 3C345 (Zensus *et al.* 1995), M87 (Biretta 1993). Since jets are unlikely to be ejected from the surface of compact objects, therefore, it has to originate from accreting matter.

High luminosity and broad band spectra from AGNs, favour the model of accretion of matter and energy on to a super massive ($10^6\text{--}9M_{\odot}$) black hole as the prime mover. The same line of reasoning also led to the conclusion that X-ray binaries harbour neutron stars or stellar mass ($\lesssim 10M_{\odot}$) black holes at the centre, while the secondary star feeds the compact object. Many of the black hole (BH) X-ray binaries are observed to go through a stage, in which relativistic twin jets are ejected and resemble scaled down version of AGN or quasar jets; as a result, these sources have been coined micro-quasars (Mirabel *et al.* 1992). Accretion of matter on to a compact object explains the luminosities and spectra of AGNs and micro-quasars, but can accretion be linked with the formation of jets? Interestingly, simultaneous radio and X-ray observations of micro-quasars show a very strong correlation between the spectral states of the accretion disc and the associated jet states (Gallo *et al.* 2003; Fender *et al.* 2010; Rushton *et al.* 2010), which reaffirms the fact that jets do originate from the accretion disc. Although this type of spectral state changes and the related change in jet states have not been observed for AGNs, however, the very fact that the timescales of AGNs and micro-quasars can be scaled by the central mass (McHardy *et al.* 2006), we expect similar correlation of spectral and jet states in AGNs too. Working with the central idea that jets are launched from accretion discs, a natural question arises, i.e., which part of the disc is responsible for jet generation. Recent observations have shown that jets originate from a region which is less than 100 Schwarzschild radius (r_s) around the unresolved central object (Junor *et al.* 1999; Doeleman *et al.* 2012), which implies that the entire disc may not participate in formation of jets, but only the central region of the disc is responsible.

Again by invoking the similarity of AGNs and micro-quasars (McHardy et. al. 2006), one may conclude that the jet originates from a region close to the central compact object for micro-quasars too. This also finds indirect support from observations of various micro quasars. Observations showed that the jet activity starts when the object is in low-hard state (LHS i. e., when the disc emission maximizes in hard, or, high energy X-rays but the over all luminosity is low). The jet strength increases as accretion disc becomes luminous in the intermediate hard states (IHS) and eventually with a surge in disc luminosity and after relativistic ejections, the accretion disc goes into high soft state (HSS i. e., disc emission maximizes in soft X-rays but luminous). No jet activity has been observed in HSS. This cycle is repeated as some kind of hysteresis and is known as hardness-intensity-diagram or HID (Fender *et al.* 2004). This indirectly suggests that the component of the disc which emits hard X-rays, or a compact corona, may also be responsible for jet activity. Since hard X-rays are emitted by hot electron clouds closer to the compact object, it indirectly points out that the jet originates from a region close to the BH even for micro-quasars.

Earliest model of accretion disc was the Keplerian disc or KD (disc with Keplerian angular momentum distribution and optically thick along the radial direction, see Shakura & Sunyaev 1973; Novikov & Thorne 1973). KD explained the thermal part of the BH accretion disc spectra, but could not explain the non-thermal part of it. This deficiency in the KD, prompted the emergence of many accretion disc models like thick disc (Paczynski & Wiita 1980), advection dominated accretion flow (Narayan *et al.* 1997), advective discs (Liang & Thompson 1980; Fukue 1987a; Chakrabarti 1989; Chattopadhyay & Chakrabarti 2011). Whatever, may be the accretion disc models, observation of strong correlation of the X-ray data (arising from convergent flow and therefore accretion) and radio data (originating from the outflowing jets) in microquasars, and the associated timing properties, also imposed some constraints on the disc-jet system. In micro quasars it was observed that the hard photons oscillate in a quasi periodic manner and which evolves from low values in LHS to high values in the intermediate states, and disappears in the HSS. This suggests that a compact corona is favourable, than an extended one, since it would be easier to oscillate a compact corona than an extended one. It was also suggested that the extended corona cannot explain the spectra of X-ray binaries in the LHS (Dove et. al. 1997; Gierlinski et. al. 1997). So from observations, one can summarize about three aspects of jet and accretion discs: they are (i) direct observation of inner region of M87 jet shows, the jet base is close to the central object; (ii) corona emits non-thermal emission, and the HSS state has very weak or no signature of

corona, as well as, the existence of jets and (iii) the corona is also compact in size. So it is quite possible that, corona is probably the base of the jet, or, a significant part of the jet base.

Unfortunately, the accretion disc around a BH has not been resolved and only the jet has actually been observed, therefore, studying the visible part of the jet is also an integral part of reconstructing the entire picture, and hence jets, especially the AGN jets are intensely investigated. Generally, it is assumed that jets from AGNs are ultra-relativistic with terminal Lorentz factors $\gamma_\infty \gtrsim 10$. However, with the discovery of more AGNs and increasingly precise observations, these facts are slowly being challenged now. On one hand, for BL Lac PKS 2155-304 the estimated terminal Lorentz factor is truly relativistic i. e., easily $\gamma_\infty \gtrsim 10$ (Aharonian *et al.* 2007), on the other hand, spectral fitting of NGC 4051 requires a more moderate range of Lorentz factors (Maitra *et al.* 2011). Infact, for FRI type jet 3C31, which has well resolved jet and counter jet observations, the jet terminal speed is $v_\infty \sim 0.8c \rightarrow 0.85c$ (c the speed of light) and then slowing down to $\sim 0.2c$ at few kpc due to entrainment with ambient medium (Laing & Bridle 2002). This implies that jets of AGNs comes at a variety of strength, length and terminal speeds (v_∞), somewhat similar to those around microquasars. For example in microquasars, SS433 jet shows a quasi-steady jet with $v_\infty \sim 0.26c$ (Margon 1984), while GRS1915+105 jet is truly relativistic (Mirabel & Rodriguez 1994). Not only that, terminal speeds estimated for a single micro-quasar may vary in different outbursts (Miller *et al.* 2012). In other words, astrophysical jets around compact objects are relativistic, but the terminal speed may vary from being mildly relativistic to ultra-relativistic. Therefore, acceleration mechanism must be multi-staged and may be result of many accelerating processes like magnetic fields and radiation driving (Sikora & Wilson 1981; Ferrari *et al.* 1985; Fukue 1996, 2000; Fukue *et al.* 2001; Vlahakis & Tsinganos 1999; Chattopadhyay & Chakrabarti 2002a,b; Chattopadhyay *et al.* 2004; Chattopadhyay 2005; Kumar *et al.* 2014; Vyas *et al.* 2015).

Estimation of bulk jet speeds from AGN jets are mostly inferred from complicated observational data. Often, the presence of bright jet in comparison to dim counter jet, are believed to constrain the bulk speed of the jet (Wardle & Aaron 1997). It has also been noted above that bulk speed required to fit the observed data, also gives us an estimate of the bulk speed of the jet (Laing & Bridle 2002). Many of these jets have knots and hot spots, which are regions of enhanced brightness. Some of these knots exhibit superluminal speeds (Biretta *et al.* 1999), which give us an estimate of the bulk speed of the knots and the under-

lying jet speed. These knots and hot spots are thought to arise due to the presence of shocks in the jet beam, due to its interaction with the ambient medium. These shocks then create high energy electrons by shock acceleration and produce non-thermal, high energy photons. By analyzing multi-wavelength data of the M87 jet, Perlman & Wilson (2005) concluded that external shocks fit this general idea pretty well. From the accumulated knowledge of hydrodynamic simulations, we know that these shocks form as a result of interaction with the ambient medium (Marti et. al. 1997) and therefore they form at large distances from the central object. However, internal shocks by faster jet blobs following slower ones, may catch up and produce internal shocks close ($\sim 100r_s$) to the central BH (Kataoka et. al. 2001), which was seen in some simulations of accretion-ejection system (Lee et. al. 2016). However, it is not plausible to form shocks closer to the jet base by this process, because the leading blob and the one following, both possess different but relativistic speeds, so a significant distance has to be traversed before they collide. Is it at all possible to form shocks in the jet much closer to the central object?

As jets are supposed to originate close to the central object and from the accreting matter, therefore the jet base should be subsonic. Since the jets are observed when they are actually far from the central object and traveling at a very high speed, therefore, one can definitely say that these jets are transonic (transits from subsonic to supersonic) in nature. We know conical flows are smooth monotonic functions of distance, or in other words, cross the sonic point only once (Michel 1972; Blumenthal & Mathews 1976; Chattopadhyay & Ryu 2009). Since the base of the jet is very hot, it would be expanding very fast, and there would be very little resistance to the outflowing jet to force it to deviate from its conical trajectory. However, if the jet is flowing through intense radiation field, then the jet would see a fraction of the radiation field approaching it, and might get slowed down, to form multiple sonic point (Vyas *et al.* 2015) and even shock (Ferrari *et al.* 1985). It is also to be noted that, most of the theoretical investigations on jets were conducted in special relativistic regime, including Ferrari *et al.* (1985) and Vyas *et al.* (2015). The reason being that, the distances from the central BH at which the jets are observed, the effect of gravity is negligible but the bulk speed is relativistic. And in order to limit the forward expansion of the jet, a Newtonian form of gravitational potential was added adhoc in the special relativistic equations of motion (Ferrari *et al.* 1985; Fukue 1996; Chattopadhyay 2005; Vyas *et al.* 2015). Newtonian (or, pseudo-Newtonian) gravitational potential is incompatible with special relativity which can be argued from the equivalence principle itself. But, if we choose not to be too fussy, even

then, gluing special relativity and gravitational potentials destroy the constancy of Bernoulli parameter in absence of dissipation, in other words, we compromise one of the constants of motion. Moreover, Ferrari *et al.* (1985) obtained spiral type sonic points, and we know that spiral type sonic points are obtained in presence of dissipation. Is this the direct fall out of combining Newtonian potential with special relativity? Therefore, we chose Schwarzschild metric, in order to consider gravity properly. But in keeping with most of the investigations of jet (Fukue 1987b; Memola *et al.* 2002; Falcke 1996), no particular accretion disc model is used to launch the jet. Furthermore, radial outflows do not show any multiplicity of sonic points, then what should generate multiple sonic points in jets. Does accretion disc shape the jet in such a fashion? In addition, most of the attempts on obtaining jet solutions were conducted in the domain of fixed adiabatic index (Γ) equation of state for jet fluid. How would a relativistic and therefore variable Γ equation of state of the gas affect the solution? What would be the possible effect of composition in the jet. In this paper, we would address these issues in details.

In section 2 we present simplifying assumptions, governing equations. In section 3, we outline the process of generating solutions along with detailed discussion on nature of sonic points and shock conditions. Then we present results in section 4 and finally conclude the analysis in section 5.

2 ASSUMPTIONS, GOVERNING EQUATIONS AND JET GEOMETRY

Since the present study is aimed at studying jet starting very close to the central object, general relativity is invoked. We choose the simplest metric, *i.e.*, Schwarzschild metric, which describes curved space-time around a non-rotating BH, and is given by

$$ds^2 = - \left(1 - \frac{2GM_B}{c^2 r}\right) c^2 dt^2 + \left(1 - \frac{2GM_B}{c^2 r}\right)^{-1} dr^2 + r^2 d\theta^2 + r^2 \sin^2 \theta d\phi^2, \quad (1)$$

where r , θ and ϕ are usual spherical coordinates, t is time and M_B is the mass of the central black hole. In the rest of the paper, we use geometric units where $G = M_B = c = 1$, so that the units of length and time are $r_g = GM_B/c^2$ and $t_g = GM_B/c^3$, respectively. In this system of units, the Schwarzschild radius, or the radius of the event horizon is $r_s = 2$. Although in the rest of the paper, we express the equations in the geometric units (until specified otherwise), we choose to retain the same representation for the coordinates as in equation (1). The fluid jet is considered to be in steady state (*i.e.*, $\partial/\partial t = 0$). Further, as the jets are collimated, we consider an on axis (*i.e.*, $u^\theta = u^\phi = \partial/\partial\theta = 0$) and axis-symmetric

($\partial/\partial\phi = 0$) jet. Effects of radiation and magnetic field as dynamic components are being ignored for simplicity. If the jet is very hot at the base, then radiation driving near the base will be ineffective (Vyas *et al.* 2015). In powerful jets, magnetic fields are likely to be aligned with the local velocity vector and hence the magnetic force term will not arise (similar to coronal holes, see Kopp & Holzer 1976). Therefore, up to a certain level of accuracy, and in order to simplify our treatment, we ignore radiation driving and magnetic fields in the present paper and effects of these will be dealt elsewhere. In the advective disc model, the inner funnel or post-shock disc (PSD) acts as the base of the jet (Chattopadhyay & Das 2007; Kumar & Chattopadhyay 2013; Kumar *et al.* 2014; Kumar & Chattopadhyay 2014; Das *et al.* 2014; Chattopadhyay & Kumar 2016; Lee *et al.* 2016) and also the Comptonizing corona (Chakrabarti & Titarchuk 1995). The shape of the PSD is torus (see simulations Das *et al.* 2014; Lee *et al.* 2016) and its dimension is about $\gtrsim \text{few} \times 10r_g$. Therefore, launching the jet inside the torus shaped funnel, simultaneously satisfies the observational requirement that the corona and the base of the jet be compact. Having said so, we must point out that, we actually do not obtain the jet input parameters (E & \dot{M}) from advective accretion disc solutions, but the input parameters are supplied. This implies, any accretion disc model with compact torus like hot corona will satisfy the underlying disc model. However, advective disc model with PSD gets a special mention because possibility of hot electron distribution close to the central object, is inbuilt to the model. The only role of the disc considered here, is to confine the jet flow boundary at the base, for one of the jet model (M2) considered in this paper. Since the exact method of how the jet originates from the disc is not being considered in this paper, so the jet input parameters are actually free parameters independent of the disc solutions. This paper is an exploratory study of the role of jet flow geometry close to the base, on jet solutions and therefore we present all possible jet solutions.

Observations show that the core temperatures of powerful AGN jets are estimated to be quite high (Moellenbrock *et al.* 1996). So the jets are hot to start with in this paper too. The advective disc model, as in most disc models, do come with a variety of inner disc temperatures. Simulations of advective discs for high viscosity parameter produced $T \gtrsim 10^{12}\text{K}$ in the PSD (Lee *et al.* 2016). Moreover in presence of viscous dissipation in curved space-time, the Bernoulli parameter ($-hu_t$) may increase by more than 20% of its value at large distance and produce very high temperatures in the PSD (Chattopadhyay & Kumar 2016). For highly rotating BHs too, the temperatures of the inner disc easily approaches 10^{12} K. It must also

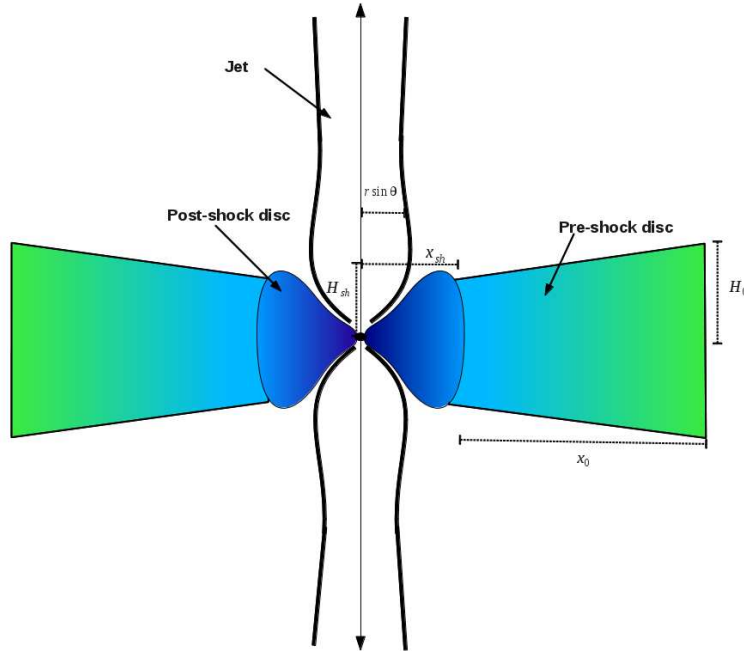


Figure 1. Cartoon diagram of accretion disc-jet geometry of model M2. The pre-shock and the post-shock disc are shown. On the figure we mark the shock location x_{sh} , half-height of the shock H_{sh} , the outer edge of the disc x_o and half height at x_o is H_o .

be remembered that inner regions of the accretion disc can be heated by Ohmic dissipation, reconnection, turbulence heating or MHD wave dissipation may heat up the inner disc or the base of the jet (Beskin 2003). High temperatures in the accretion disc can induce exothermic nucleosynthesis too (Chakrabarti et. al. 1987; Hu & Peng 2008). All these processes taken together in an advective disc will produce very hot jet base. We do not specify the exact processes that will produce very hot jet base, but would like to emphasize that it is quite possible to achieve so. One may also wonder, that if the jets are indeed launched from the disc, how justified is it to consider non-rotating jets. Phenomenologically speaking, if jets have a lot of rotation then it would not flow around the axis of symmetry and therefore, either it has to be launched with less angular momentum or, has to lose most of the angular momentum with which it is launched. It has been shown that viscous transport removes significant angular momentum of the collimated outflow close to the axis (Lee et. al. 2016). Since the jet is launched with low angular momentum and it is further removed by viscosity or by the presence of magnetic field, therefore, the assumption of non-rotating hot jet is quite feasible. Incidentally, similar to this study, there are many theoretical studies of jets which have been undertaken under similar assumptions of non-rotating, hot jets at the base (Fukue 1987b; Memola et. al. 2002; Falcke 1996).

2.1 Geometry of the jet

Observations of extra-galactic jets show high degree of collimation, so it is quite common in jet models to consider conical jets with small opening angle. We considered two models of jets, the first model being a jet with conical cross-section and we call this model as M1. However, the jet at its base is very hot and subsonic, and since the pressure gradient is isotropic, the jet will expand in all directions. The walls of the inner funnel of the PSD will provide natural collimation of the jet flow near its base. If the base of the jet is very energetic, then it is quite likely to become transonic within the funnel of the PSD (see Fig. 1). In a magneto-hydrodynamic simulations of jets, Kudoh *et al.* (2002) showed that the jet indeed flows through the open field line region, but at a certain distance above the torus shaped disc, the jet surface is pushed towards the axis and beyond that the jet expands again, resulting into a converging-diverging cross-section. The cross-section adopted for Model M2 in this paper, is inspired by these kinds of jet simulations. We ensured that the variation of the geometry of M2 is smooth and slowly varying, such that the solutions are not crucially dependent on the particular shape of the flow geometry.

The general form of jet cross section or, $\mathcal{A}(r)$ is

$$\mathcal{A} = \mathcal{G}r^2, \quad \text{where, } \mathcal{G} = 2\pi(1 - \cos\theta); \quad \theta \text{ is polar angle at } r \quad (2)$$

For the first model M1:

$$\cos\theta = \frac{-(Cm)/r + \sqrt{-C^2/r^2 + m^2 + 1}}{(m^2 + 1)}, \quad (3)$$

where, C and $m(= \tan\theta_0)$ are the constant intercept and slope of the jet boundary with the equatorial plane, with θ_0 being the constant opening angle with the axis of the jet. The value of the constant intercept might be $C = 0$ or $C \neq 0$, either way, the solutions are qualitatively same and we take $C = 0$.

The second model M2 mimics a geometry whose outer boundary is the funnel shaped surface of the accretion disc at the jet base i. e., $d\mathcal{A}/dr > 0$ (see, Fig. B1a). As the jet leaves the funnel shaped region of PSD, the rate of increase of the cross-section gets reduced $d\mathcal{A}/dr \sim 0$. It again expands and finally becomes conical at large distances, where $d\mathcal{A}/dr \propto r$. The functional form of r and θ of the jet geometry for the model M2 is given by,

$$r \sin\theta = \frac{k_1 d_1 (r - n)}{1 + d_2 (r - n)^2} + m_\infty (r - n) + k_2, \quad (4)$$

where, $k_1 = 5x_{\text{sh}}/\pi$, $k_2 = x_{\text{sh}}/2$, $d_1 = 0.05$, $d_2 = 0.0104$, $m_\infty = 0.2$ and $n = 5$. A schematic diagram of the geometry of the M2 jet model and disc is shown in Fig. 1, where x_{sh} is the

shock in accretion, or in other words, the length scale of the inner torus like region. In Eq. (4), k_1, k_2 are parameters which influence the shape of jet geometry at the base, while d_1, d_2, m_∞ and n are constants, which together with k_1 and k_2 , shape the jet geometry. Here, we assume at large distances the jet is conical and $m_\infty (= \tan \theta_\infty)$ is the gradient which corresponds to the terminal opening angle to be 11° . The size of the PSD or x_{sh} influences the jet geometry and the jet geometry at the base is shaped by the shape of the PSD as shown in appendix (B). A typical jet geometry for a given set of accretion solution is plotted in Fig. B1.

2.2 Equations of motion of the jet

2.2.1 Equation of state

Hydrodynamic equations of motion are solved with the help of a closure relation between internal energy density, pressure and mass density (e, p, ρ , respectively) of the fluid, called the equation of state (EoS). An EoS for multispecies, relativistic flow proposed by Chattopadhyay (2008); Chattopadhyay & Ryu (2009) is adopted, and is given by,

$$e = n_{e^-} m_e c^2 f, \quad (5)$$

where n_{e^-} is the electron number density and f is given by

$$f = (2 - \xi) \left[1 + \Theta \left(\frac{9\Theta + 3}{3\Theta + 2} \right) \right] + \xi \left[\frac{1}{\eta} + \Theta \left(\frac{9\Theta + 3/\eta}{3\Theta + 2/\eta} \right) \right]. \quad (6)$$

Here, non-dimensional temperature is defined as $\Theta = kT/(m_e c^2)$, k is the Boltzmann constant and $\xi = n_{p^+}/n_{e^-}$ is the relative proportion of protons with respect to the number density of electrons. The mass ratio of electron and proton is $\eta = m_e/m_{p^+}$. It is easy to see that by putting $\xi = 0$, we generate EoS for relativistic $e^- - e^+$ plasma (Ryu *et al.* 2006). The expressions of the polytropic index N , adiabatic index Γ and adiabatic sound speed a are given by

$$N = \frac{1}{2} \frac{df}{d\Theta}; \quad \Gamma = 1 + \frac{1}{N}; \quad a^2 = \frac{\Gamma p}{e + p} = \frac{2\Gamma\Theta}{f + 2\Theta}. \quad (7)$$

This EoS is an approximated one, and the comparison with the exact one shows that this EoS is very accurate (Appendix C of Vyas *et al.* 2015). Additionally, being algebraic and avoiding the presence of complicated special functions, this EoS is very easy to be implemented in simulation codes, as well as, be used in analytic investigations (Chattopadhyay & Ryu 2009; Chattopadhyay & Chakrabarti 2011; Ryu *et al.* 2006; Chattopadhyay *et al.* 2013).

2.2.2 Equations of motion

The energy momentum tensor of the jet matter is given by

$$T^{\alpha\beta} = (e + p)u^\alpha u^\beta + pg^{\alpha\beta} \quad (8)$$

where the metric tensor components are given by $g^{\alpha\beta}$ and u^α represents four velocity.

The equations of motion are given by

$$T_{;\beta}^{\alpha\beta} = 0 \quad \text{and} \quad (\rho u^\beta)_{;\beta} = 0, \quad (9)$$

The first of which is energy-momentum conservation equation and second is continuity equation. From the above equation, the i^{th} component of the momentum conservation equation is obtained by operating the projection tensor on the first of equation (9), *i.e.*,

$$(g_\alpha^i + u^i u_\alpha) T_{;\beta}^{\alpha\beta} = 0 \quad (10)$$

Similarly, the energy conservation equation is obtained by taking

$$u_\alpha T_{;\beta}^{\alpha\beta} = 0 \quad (11)$$

For an on-axis jet, equations (10, 11) becomes;

$$u^r \frac{du^r}{dr} + \frac{1}{r^2} = - \left(1 - \frac{2}{r} + u^r u^r \right) \frac{1}{e + p} \frac{dp}{dr}, \quad (12)$$

$$\frac{de}{dr} - \frac{e + p}{\rho} \frac{d\rho}{dr} = 0, \quad (13)$$

While the second of equation (9) when integrated becomes mass outflow rate equation,

$$\dot{M}_{\text{out}} = \rho u^r \mathcal{A}. \quad (14)$$

Here, \mathcal{A} is the cross-section area of the jet. The differential form of the outflow rate equation is,

$$\frac{1}{\rho} \frac{d\rho}{dr} = - \frac{1}{\mathcal{A}} \frac{d\mathcal{A}}{dr} - \frac{1}{u^r} \frac{du^r}{dr}. \quad (15)$$

By using equation (14), pressure p can be given as

$$p = \frac{2\Theta\rho}{\tau} = \frac{2\Theta\dot{M}_{\text{out}}}{\tau u^r \mathcal{A}} \quad (16)$$

Here \mathcal{A} is the cross section of the jet (section 2.1) and $\tau = (2 - \xi + \xi/\eta)$. Equations (12-13), with the help of equation (15), are simplified to

$$\gamma^2 v \left(1 - \frac{a^2}{v^2} \right) \frac{dv}{dr} = \left[a^2 \left\{ \frac{1}{r(r-2)} + \frac{1}{\mathcal{A}} \frac{d\mathcal{A}}{dr} \right\} - \frac{1}{r(r-2)} \right] \quad (17)$$

and

$$\frac{d\Theta}{dr} = -\frac{\Theta}{N} \left[\frac{\gamma^2}{v} \left(\frac{dv}{dr} \right) + \frac{1}{r(r-2)} + \frac{1}{\mathcal{A}} \frac{d\mathcal{A}}{dr} \right] \quad (18)$$

Here the three-velocity v is given by $v^2 = -u_i u^i / u_t u^t = -u_r u^r / u_t u^t$, *i.e.*, $u^r = \sqrt{g^{rr}} \gamma v$ and $\gamma^2 = -u_t u^t$ is the Lorentz factor. All the information like jet speed, temperature, sound speed, adiabatic index, polytropic index as functions of spatial distance, can be obtained by integrating equations (17-18).

A comparison with De Laval Nozzle helps us to understand the nature of the equations and the expected nature of the solutions. The non-relativistic version of De Laval Nozzle (DLN) is obtained by considering $v \ll 1$ and $r \rightarrow$ large in equation (17), which means the first and the third term in r. h. s drop off and $\gamma \rightarrow 1$, but for the special relativistic (SR) version there is no constrain on γ . In the subsonic regime ($v < a$), the jet will accelerate if $d\mathcal{A}/dr < 0$ (converging cross-section), both in the non-relativistic and in SR version of DLN problem. While in the supersonic regime ($v > a$) the jet accelerate if $d\mathcal{A}/dr > 0$ (expanding cross-section), and forms the sonic point where $d\mathcal{A}/dr = 0$. Therefore, a pinch in the flow geometry (*i. e.*, a convergent-divergent cross section) makes a subsonic flow to become transonic. However, in presence of gravity, the first and the third terms cannot be ignored. The third term is the purely gravity term, while the first term is the coupling between gravity and the thermal term. Therefore, the gravity and the flow's thermal energy now compete with the cross-section term to influence the jet solution. The third term is negative, the first term is positive definite, the middle term may either be positive or negative. However, near the horizon the third dominates the other two and even for a conical flow ($d\mathcal{A}/dr > 0$), the r. h. s of equation (17) will be negative. Hence a subsonic jet will accelerate up to the sonic point r_c , where r. h. s becomes zero. For $r > r_c$ the flow is supersonic and still the jet accelerates because at those distances the r. h. s of equation (17) is positive. Therefore, unlike the typical DLN problem, in presence of gravity, it is not mandatory that $d\mathcal{A}/dr = 0$ so that an r_c may form, *i. e.*, gravity ensures the formation of the sonic point. But if the magnitude of $d\mathcal{A}/dr$ changes drastically, even without changing sign, the interplay with the gravity term may ensure formation of multiple sonic points.

A physical system becomes tractable when solutions are described in terms of their constants of motion. Using a time like Killing vector $\zeta_\nu = (1, 0, 0, 0)$, the equation of motion (equation 9) becomes,

$$(T^{\mu\nu} \zeta_\nu)_{;\mu} = J_{;\mu}^\mu = 0;$$

$$\text{or, } \left(\sqrt{-g} J^r \right)_{,r} = \left(r^2 \sin\theta T_t^r \right)_{,r} = 0.$$

Integrating the above equation, we obtain the negative of the energy flux as a constant of motion,

$$\mathcal{A}(e + p)u^r u_t = -\dot{E} = \text{constant} \quad (19)$$

The relativistic Bernoulli equation or, the specific energy of the jet, is obtained by dividing equation (19) by equation(14)

$$E = \frac{\dot{E}}{\dot{M}_{\text{out}}} = -hu_t. \quad (20)$$

Here, $h = (e + p)/\rho = (f + 2\Theta)/\tau$ is the specific enthalpy of the fluid and $u_t = -\gamma\sqrt{(1 - 2/r)}$.

The kinetic power of the jet is the energy flux through the cross-section

$$L_j = \dot{E} = \dot{M}_{\text{out}} E \quad (21)$$

If only the entropy equation (13) is integrated, then we obtain the adiabatic relation which is equivalent to $p \propto \rho^\Gamma$ for constant Γ flow (Kumar *et al.* 2013),

$$\rho = \mathcal{C} \exp(k_3) \Theta^{3/2} (3\Theta + 2)^{k_1} (3\Theta + 2/\eta)^{k_2}, \quad (22)$$

where, $k_1 = 3(2 - \xi)/4$, $k_2 = 3\xi/4$, $k_3 = (f - \tau)/(2\Theta)$ and \mathcal{C} is the constant of entropy.

If we substitute ρ from the above equation into equation (14), we get the expression for entropy-outflow rate (Kumar *et al.* 2013),

$$\dot{\mathcal{M}} = \frac{\dot{M}_{\text{out}}}{\text{geom.const.}\mathcal{C}} = \exp(k_3) \Theta^{3/2} (3\Theta + 2)^{k_1} (3\Theta + 2/\eta)^{k_2} u^r \mathcal{A} \quad (23)$$

Equations (23) and (20) are measures of entropy and energy of the flow that remain constant along a streamline. However, at the shock, there is a discontinuous jump of $\dot{\mathcal{M}}$.

3 SOLUTION METHOD

3.1 Sonic point conditions

Jets originate from a region in the accretion disc, which is close to the central object, where, the jet is subsonic and very hot. The thermal gradient being very strong, works against the gravity and power the jet to higher velocities and in the process, v crosses the local sound speed a at the sonic point r_c , which makes the jet supersonic. The sonic point is also a critical point because, at r_c equation (17) takes the form $dv/dr \rightarrow 0/0$. This gives us the sonic point conditions,

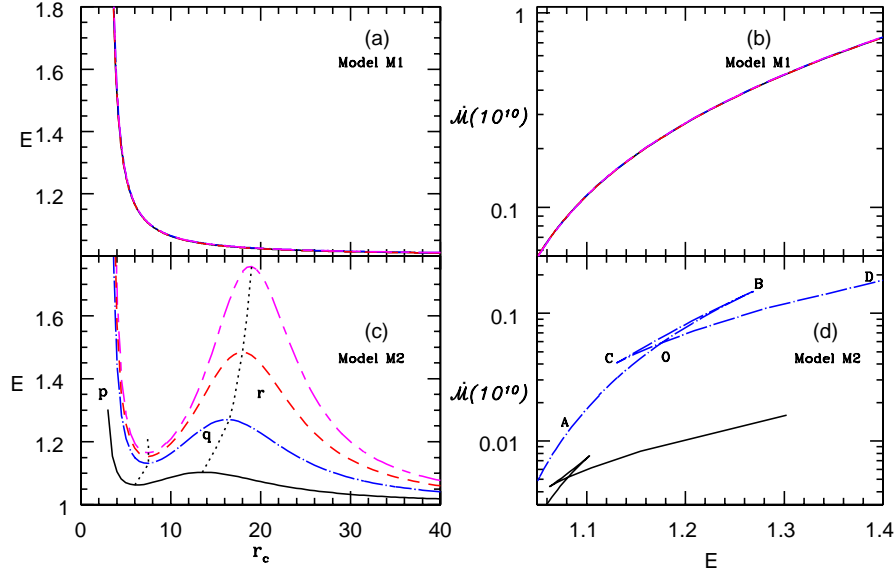


Figure 2. Variation of E with r_c (a, c) and \dot{M} with E (b, d) for the two models M1 (a, b) and M2 (c, d). Each curve represent $x_{sh} = 12$ (long-short dash, magenta), 10 (dash, red), 7 (dash-dot, blue), 3 (solid, black). (d) $\dot{M}(r_c)$ - $E(r_c)$ are plotted for only two $x_{sh} = 3$ (solid, black) and $x_{sh} = 7$ (dash-dot, blue). The composition of the jet is for $\xi = 1.0$.

$$v_c = a_c \quad (24)$$

$$a_c^2 = \left[1 + r_c(r_c - 2) \left(\frac{1}{\mathcal{A}} \frac{d\mathcal{A}}{dr} \right)_c \right]^{-1} \quad (25)$$

The $dv/dr|_c$ is calculated by employing the L'Hospital's rule at r_c and solving the resulting quadratic equation for $dv/dr|_c$. The quadratic equation can admit two complex roots leading to the either O type (or 'centre' type) or 'spiral' type sonic points, or two real roots but with opposite signs (called X or 'saddle' type sonic points), or real roots with same sign (known as nodal type sonic point).

So for a given set of flow variables at the jet base, a unique solution will pass through the sonic point(s) determined by the entropy \dot{M} and energy E of the flow. Model M1 is independent of the shock location x_{sh} in the accretion disc, but model M2 depends on x_{sh} . In Figs. (2a, b), we plot the sonic point properties of the jet for model M1, and in Figs. (2c, d) we plot the sonic point properties of M2. Each curve is plotted for $x_{sh} = 12$ (long-short dash, magenta), 10 (dash, red), 7 (dash-dot, blue), 3 (solid, black). The Bernoulli parameter of the jet E is plotted as a function of r_c in Fig. (2a, c). In Fig. (2b, d), \dot{M} is plotted as a function of E at the sonic points. The jet model M1 is a conical flow and therefore, is

independent of the accretion disc geometry. So, curves corresponding to various values of x_{sh} coincide with each other in Figs. 2a and b. Moreover, both E and $\dot{\mathcal{M}}$ are monotonic functions of r_c . In other words, a flow with a given E will have one sonic point, and the transonic solution will correspond to one value of entropy, or $\dot{\mathcal{M}}$. The situation is different for model M2. As x_{sh} is increased from 3, 7, 10, 12, the E versus r_c plot increasingly deviates from monotonicity and produces multiple sonic points in larger range of E (Fig. 2c). For small values of x_{sh} the jet cross-section is very close to the conical geometry and therefore, multiplicity of sonic points is obtained in a limited range of E . It must be noted that, for a given x_{sh} , jets with very high and low values of E form single sonic points. The range of E within which multiple sonic points may form, increases with increasing x_{sh} . The reason M1 has only one r_c , is amply clear from our discussion on DLN in section 2.2.2. We know that, if r. h. s of equation (17) is zero, a sonic point is formed. Since $\mathcal{A}^{-1}d\mathcal{A}/dr = 2/r$ is always positive, the r. h. s becomes zero only due to gravity, and therefore, there is only one r_c for M1.

For M2, the cross-section near the base expands faster than a conical cross-section, therefore, the first two terms in r.h.s of equation (17) competes with gravity. As a result, the jet rapidly accelerates to cross the sonic point withing the funnel like region of PSD. But as the jet crosses the height of PSD, the expansion is arrested and at some height $\mathcal{A}^{-1}d\mathcal{A}/dr \sim 0$. If this happens closer to the jet base then the gravity will again make the r. h. s of the equation (17) zero, causing the formation of multiple sonic points. For low values of E in M2, the thermal driving is weak and so the sonic point forms at large distances. At those distances \mathcal{A} becomes almost conical and therefore, for reasons cited above, the jet has only one sonic point. If E is very high, then the strong thermal driving makes the jet transonic at a distance very close to the jet base. For such flow, the thermal driving remains strong enough even in the supersonic domain, which negates the effect of changing $d\mathcal{A}/dr$ and do not produce more sonic points. For intermediate values of E , the jet becomes transonic at slightly larger distances. For these flows, the thermal driving in the supersonic region becomes weaker and at the same time, the expansion of the jet cross section term decreases i. e., $\mathcal{A}^{-1}d\mathcal{A}/dr \sim 0$. At those distances, the gravity again becomes dominant than the other two terms, which reduce the r. h. s of equation(17) and makes it zero to produce multiple sonic points. In Fig. (2c), the maxima and minima of E is the range which admits multiple sonic points. We plotted the locus of the maxima and minima with a dotted line, and then divided the region as ‘p’, ‘q’ and ‘r’. Region ‘p’ harbours inner X-type sonic point, region

‘q’ harbours O-type sonic point and region ‘r’ harbours outer X-type sonic points. Figure (2d) is the knot diagram (similar to ‘kite-tail’ for accretion, see Kumar *et al.* 2013) between E and $\dot{\mathcal{M}}$ evaluated at r_c , for two values of $x_{\text{sh}} = 3$ (solid, black) and $x_{\text{sh}} = 7$ (dashed-dot, blue). For $x_{\text{sh}} = 7$ (dashed-dot, blue), the top flat line of the knot (BC) represents the O-type sonic points from region ‘q’ of Fig (2d). Similarly, AB represents outer X-type sonic points from the region ‘r’. And CD gives the values of E and $\dot{\mathcal{M}}$ for which only inner X-type sonic points (region ‘p’) exists. If the coordinates of the turning/end points of the curve be marked as $\dot{\mathcal{M}}_B$, E_B and so on, then it is clear that for $x_{\text{sh}} = 7$, multiple sonic points form for jet parameter $E_C \leq E \leq E_B$. At the crossing point ‘O’, the entropy of both the sonic points are same. The plot for $x_{\text{sh}} = 3$ (solid, black) is plotted as a comparison, and shows that if the shock in accretion is formed close to the central object, then multiple sonic points in jets are formed for moderate range of E , a fact also quite clear from Fig. (2c).

3.2 Shock conditions

One of the major outcomes of existence of multiple sonic points in the jet, is the possibility of formation of shocks in the flow. At the shock, the flow makes a discontinuous jump in density, pressure and velocity. The relativistic Rankine-Hugoniot conditions relate the flow quantities across the shock jump and they are (Taub 1948; Chattopadhyay & Chakrabarti 2011)

$$[\rho u^r] = 0, \quad (26)$$

$$[T^{tr}] = [(e + p)u^t u^r] = 0, \quad (27)$$

and

$$[T^{rr}] = [(e + p)u^r u^r + pg^{rr}] = 0 \quad (28)$$

The square brackets denote the difference of quantities across the shock, i.e. $[Q] = Q_2 - Q_1$ with Q_2 and Q_1 being the quantities after and before the shock respectively.

Dividing equation (27) by equation (26) and then simplifying, we obtain

$$[E] = [hu_t] = 0 \quad (29)$$

It merely states that the energy remains conserved across the shock. Further, dividing (28) by (26) and a little algebra leads to

$$\left[\sqrt{g^{rr}} \left(h\gamma v + \frac{2\Theta}{\tau\gamma v} \right) \right] = 0 \quad (30)$$

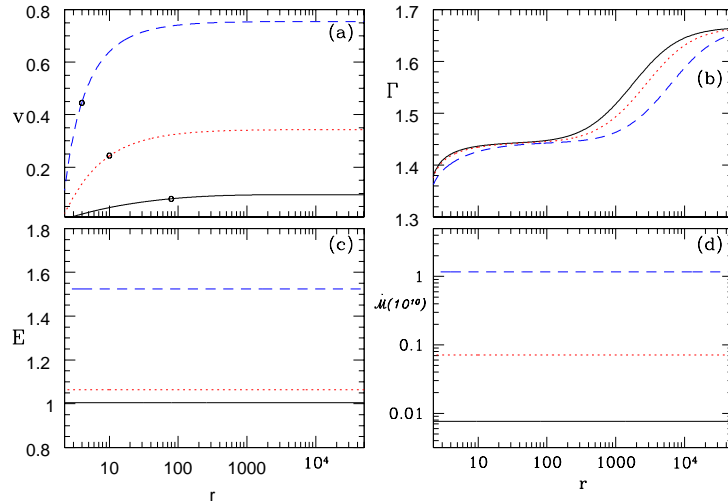


Figure 3. Model M1: Variation of (a) three velocity v , (b) adiabatic index Γ , (c) energy parameter E and (d) entropy $\dot{\mathcal{M}}$ as functions of r . The shock in accretion $x_{\text{sh}} = 12$ and flow composition $\xi = 1.0$. Each curve is characterized for $E = 1.0045$ (solid, black), $E = 1.064$ (dotted, red) and $E = 1.525$ (dashed, blue). Black open circles in (a) show the location of sonic points.

We check for shock conditions (equations 29, 30) as we solve the equations of motion of the jet. The strength of the shock is measured by two parameters compression ratio (R) and shock strength (S). R and S are ratios of densities and Mach numbers (M) across the shock (at $r = r_{\text{sh}}$). In relativistic case, according to equation (26) R is obtained as,

$$R = \frac{\rho_+}{\rho_-} = \frac{u_-^r}{u_+^r} = \frac{\gamma_- v_-}{\gamma_+ v_+}, \quad (31)$$

where, + and – stands for quantities at post-shock and pre-shock flows, respectively. Similarly, S is defined as,

$$S = \frac{M_-}{M_+} = \frac{v_- a_+}{v_+ a_-} \quad (32)$$

4 RESULTS

In this paper, we study relativistic jets flowing through two types of geometries: (i) model M1: conical jets and (ii) model M2: jets through a variable and non-conical cross-section, as described in section 2.1.

4.1 Model M1 : Conical jets

Inducting equation (3) into (2), we get a spherically outflowing jet, which, for $C = 0$ gives a constant $\theta (= \theta_0 = 11^\circ)$. The jet geometry is such that $\mathcal{A} \propto r^2$. Keeping $\xi = 1$, each curve for model M1 is plotted for $E = 1.0045$ (solid black), $E = 1.064$ (dotted red) and $E = 1.525$ (long-dashed blue) and are shown in Figs. (3a-d). Open circles denote the location of sonic

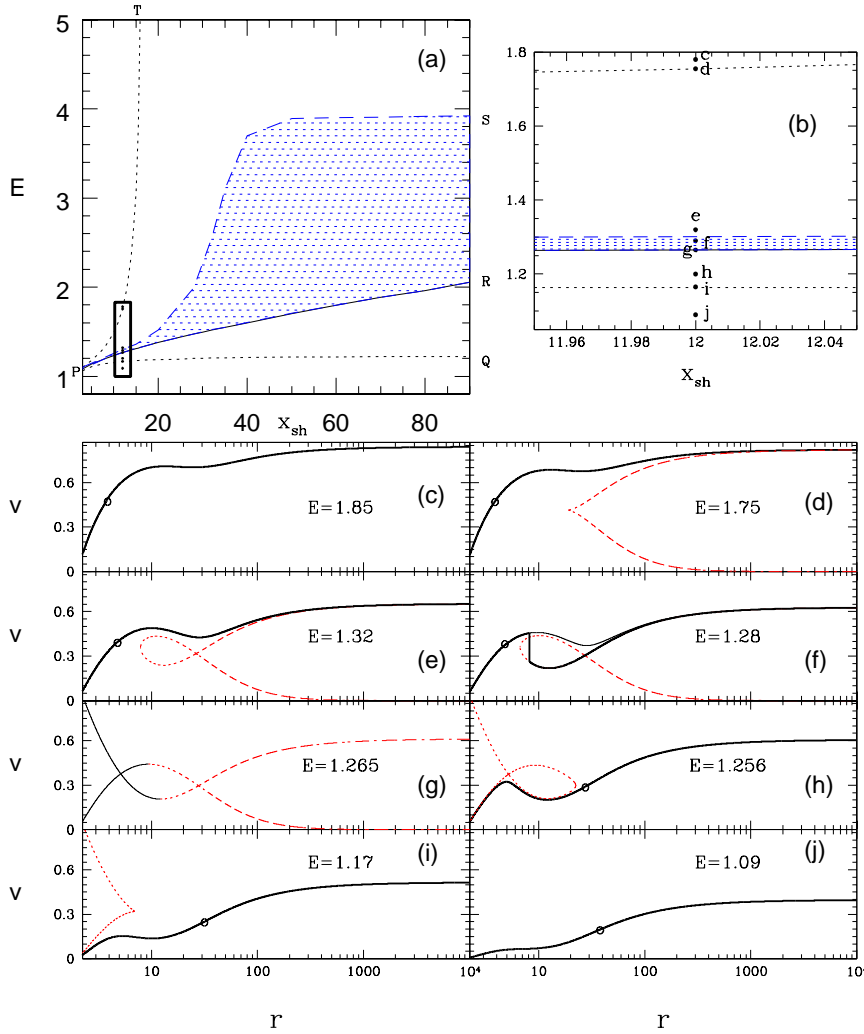


Figure 4. (a) E – x_{sh} parameter space for $\xi = 1$. PQRSTP is the region of multiple sonic point. PR is the locus of points on which the two sonic points have same entropy. Shaded region PRSP permits stable shock transition. (b) Zoomed parameter space, which shows positions ‘c’-‘j’ on $x_{\text{sh}} = 12$ for which all typical solutions are plotted in the panels (c)-(j). Circles on global solutions (solid) and as crossings in closed solutions (dashed) are the location of sonic points.

points. For higher values of E , the jet terminal speed is also higher (Fig. 3a). Higher E also produce hotter flow. So at any given r , Γ is lesser for higher E (Fig. 3b)). Since the jet is smooth and adiabatic, so E (Fig. 3c) and \dot{M} (Fig. 3d) remain constant. The variable nature of Γ is clearly shown in Fig. (3b), which starts from a value slightly above $4/3$ (hot base) and at large distance it approaches $5/3$, as the jet gets colder. As discussed in sections 2.2.2 and 3.1, for all possible parameters, this geometry gives smooth solutions with only single sonic point until and unless M1 jet interacts with the ambient medium.

4.2 Model M2

In this section, we discuss all possible solutions associated with the jet model M2. The sonic point analysis of the jet model M2 showed that for larger values of x_{sh} , multiple sonic point may form in jets for a larger range of E (Fig. 2c). In Fig. (4a), we plot the multiple sonic point region (PQRSTP) bounded by the dotted line. Dotted lines are same as those on Fig. (2c), obtained by connecting the maxima and minima of E versus r_c plot. Jets with all E , x_{sh} values within PQRSTP will harbour multiple sonic points, which is similar to the bounded region of the energy-angular momentum space for accretion disc (see, Fig. 4 of Chattopadhyay & Kumar 2016). The central solid line (PR) is the set of all E , x_{sh} which harbour three sonic points, but the entropy is same for both the inner and outer sonic points. In region QPRQ, the entropy of the inner sonic points is higher than the outer sonic point and in TPRST, it is vice versa. The zoomed part of the parameter space around $x_{\text{sh}} = 12$ is shown in (4b) and marked locations from ‘c’ to ‘j’. The solutions corresponding to the values of E (marked in Fig.4b) and $x_{\text{sh}} = 12$ are plotted in panels Fig. (4c—j). For higher energies $E = 1.85$ (> 1.75 left side of PT), only one X-type sonic point (circle) is possible close to the BH (Fig. 4c). Due to stronger thermal driving the jet accelerates and becomes transonic close to the BH. For a slightly lower $E(= 1.75)$, there are two sonic points, the solution (solid) through the inner one (shown by a small circle) is a global solution, while the second solution (dashed) terminates at the outer sonic point (crossing point) is not global (Fig. 4d). For lower E ($= 1.32$), the solution through outer sonic point is α type (dashed) and has higher entropy. An α type solution is the one which makes a closed loop at $r < r_c$ and has one subsonic and another supersonic branches starting from r_c outwards extending up to infinity (Fig. 4d). The jet matter starting from the base, can only flow out through the inner sonic point (solid), but cannot jump onto the higher entropy solution because shock conditions are not satisfied (Fig. 4e). However, for $E = 1.28$, the entropy difference between inner and outer sonic points are exactly such that, matter through the inner sonic point jumps to the solution through outer sonic point at the jet shock or r_{sh} (Fig. 4f). Solution for $E = 1.265$ is on PR and produces inner and outer sonic points with the same entropy (Fig. 4g). Figures (4c —g) are parameters lying in the TPRST. For flows with even lower energy $E = 1.256$, the entropy condition of the two physical sonic points reverses. In this case, the entropy of the inner sonic point is higher than the outer one. So, although multiple sonic points exist but no shock in jet is possible (Fig. 4h) and the jet flows out through the outer

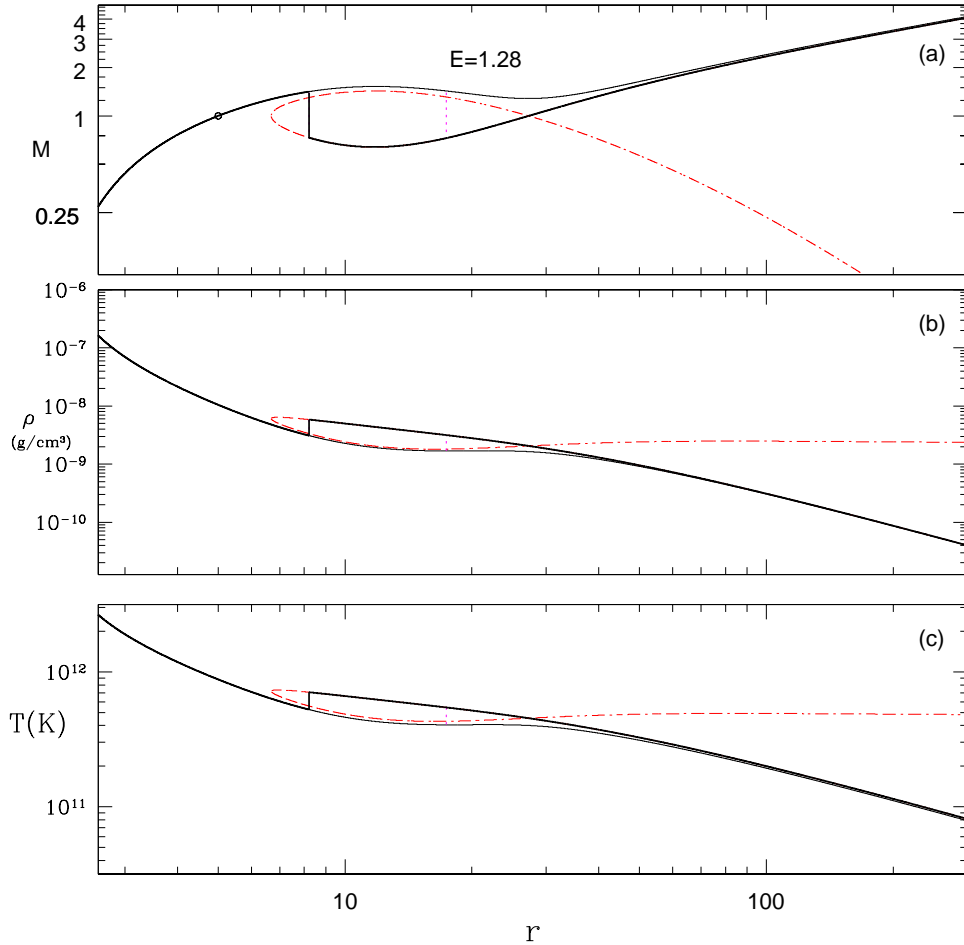


Figure 5. Variation of (a) Mach number M , (b) ρ and (c) T (in Kelvin) of a shocked jet solution. The density profile is plotted by assuming $M_{\text{BH}} = 10M_{\odot}$ and $\dot{M} = 0.01\dot{M}_{\text{Edd}}$. All the plots are obtained for $E = 1.28$.

sonic point. In Fig. (4i), the energy is $E = 1.17$ and the solution is almost the mirror image of Fig. (4d). Figures (4h, i) belong to QPRQ region. For even lower energy i. e., $E = 1.09$ a much weaker jet flows out through the only sonic point available at a larger distance from the compact object (Fig. 4j).

In Figs. 5a-c, we plot the solution of the inner region of a shocked jet, where the inner boundary values are clearly seen for a particular solution. The solid curve represents the physical solution, and the dotted curve is a possible multi valued solution which can only be accessed in presence of a jet shock. The base temperature and density (in physical units) are quite similar to the ones obtained in advective accretion disc solutions.

In the literature, many authors have studied shock in accretion discs (Fukue 1987a; Chakrabarti 1989; Chattopadhyay & Chakrabarti 2011; Chattopadhyay & Kumar 2016) and the phenomena have long been identified as the result of centrifugal barrier developing in the

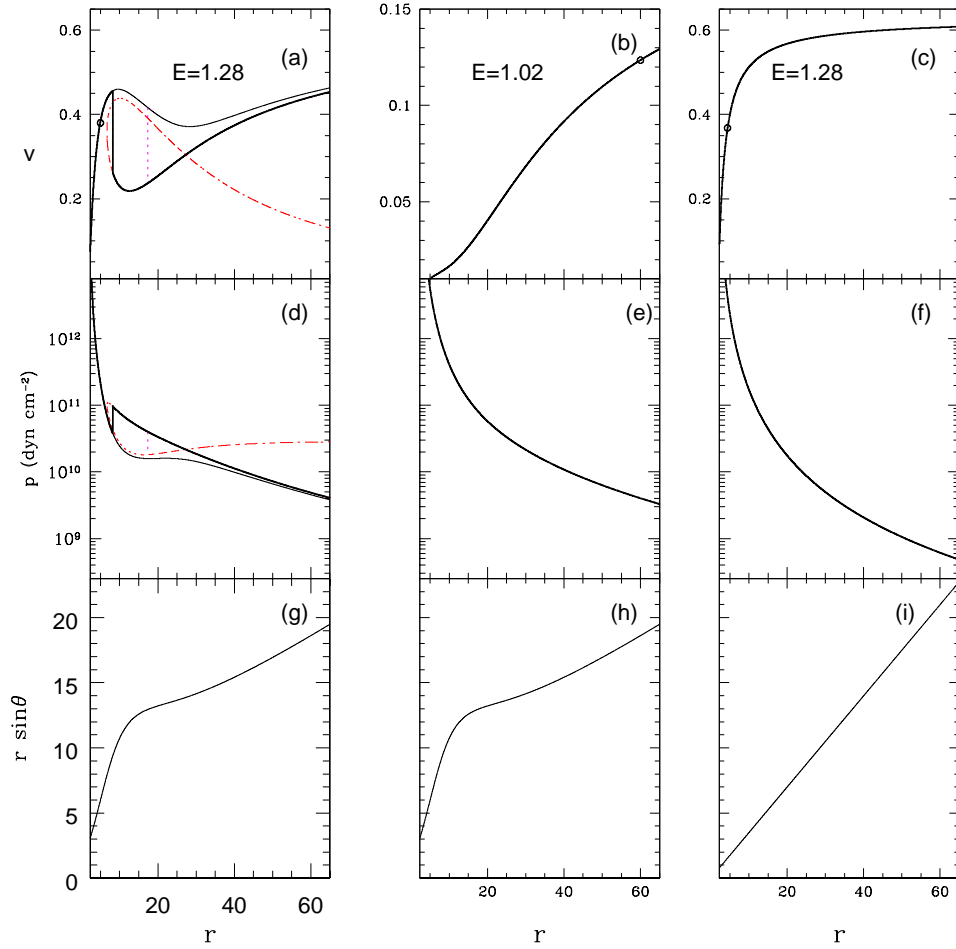


Figure 6. Three velocity v (a, b, c), pressure p in physical units (d, e, f) and jet cross section (g, h, i) are plotted as a function of r . Jet M2 are presented in the left and middle panels. Jet M1 is presented in the right panel. Thin-solid curve is a physical solution jet do not follow due to shock. Vertical lines show stable (solid) and unstable (dotted) shocks.

accreting flow. Shocks may develop in jets due to the interaction with the ambient medium, or inherent fluctuation of injection speed of the jet. But why would internal shock develop in steady jet flow, where the role of angular momentum is either absent or very weak? In Fig. 6(a), we plot velocity profile of a shocked jet solution with parameters $E = 1.28$, $\xi = 1.0$ and $x_{\text{sh}}=12$. The jet, starting with subsonic speeds at base, passes through the sonic point (circle) at $r_c = 5$ and becomes transonic. This sonic point is formed due to gravity term (third term in the r. h. s of equation 17) which is negative and equals other two terms at r_c making the r. h. s of equation (17) equal to zero. It is to be remembered that, jets with higher values of E implies hotter flow at the base, which ensures greater thermal driving which makes the jet supersonic within few r_g of the base. However, after the jet becomes supersonic ($v > a$), the jet accelerates but within a short distance beyond the sonic point the jet decelerates (thin, solid line). This reduction in jet speed occurs due to the geometry

of the flow. In Fig. (6g), we have plotted the corresponding cross section of the jet. The jet rapidly expands in the subsonic regime, but the expansion gets arrested and the expansion of the jet geometry becomes very small $\mathcal{A}^{-1}d\mathcal{A}/dr \sim 0$. Therefore the positive contribution in the r. h. s of equation (17) reduces significantly which makes $dv/dr \leq 0$. Thus the flow is decelerated resulting in higher pressure down stream (thin solid curve of Fig. 6d). This resistance causes the jet to undergo shock transition at $r_{\text{sh}} = 8.21$. The shock condition is also satisfied at $r_{\text{sh}} = 17.4$, however this outer shock can be shown to be unstable (see, Appendix A and also Nakayama 1996; Yang & Kafatos 1995; Yuan et. al. 1996). We now compare the shocked M2 jet in Fig. (6a, d, g) with two other jet flows, (i) a jet of model M2 but with low energy $E = 1.02$ (Fig. 6b, e, h); and (ii) a jet of model M1 and with the same energy $E = 1.28$ (Fig. 6c, f, i). In the middle panels, $E = 1.02$ and therefore the jet is much colder. Reduced thermal driving causes the sonic point to form at large distance (open circle in Fig. 6b). The large variations in the fractional gradient of \mathcal{A} occurs well within r_c . At $r > r_c$ $\mathcal{A}^{-1}d\mathcal{A}/dr \rightarrow 2/r$, which is similar to a conical flow. Therefore, the r. h. s of equation (17) does not become negative at $r > r_c$. In other words, flow remains monotonic. The pressure is also a monotonic function (Fig. 6e) and therefore no shock transition occurs. In order to complete the comparison, in the panels on the right (Fig. 6c, f, i), we plot a jet model of M1, with the same energy as the shocked one ($E = 1.28$). Since fractional variation of the cross section is monotonic i. e., at $r > r_c$, $\mathcal{A}^{-1}d\mathcal{A}/dr = 2/r$ (Fig. 6i), the all jet variables like v (Fig. 6c) and pressure (Fig. 6f) remains monotonic. No internal shock develops.

Therefore to form such internal shocks in jets, the jet base has to be hot in order to make it supersonic very close to the base. And then the fractional gradient of the jet cross section needs to change rapidly, in order to alter the effect of gravity, so that the jet beam starts resisting the matter following it and form a shock.

Figures (6a-i) showed that departure of the jet cross section from conical geometry is not enough to drive shock in jet. It is necessary that the jet becomes transonic at a short distance from the base and a significant fractional change in jet cross-section occurs in the supersonic regime of the jet. Since the departure of the jet cross-section from the conical one, depends on shape of the inner disc, or in other words, the location of the shock in accretion, we study the effect of accretion disc shock on the jet solution. We compare jet solutions (i. e., v versus r) for various accretion shock locations for e. g., $x_{\text{sh}} = 90$ (Fig. 7a), $x_{\text{sh}} = 40$ (Fig. 7b), $x_{\text{sh}} = 15$ (Fig. 7c) and $x_{\text{sh}} = 9$ (Fig. 7d). In Figs. (4c-i), all possible solutions were obtained by keeping x_{sh} constant for different values of E . In Figs. (7a-d)

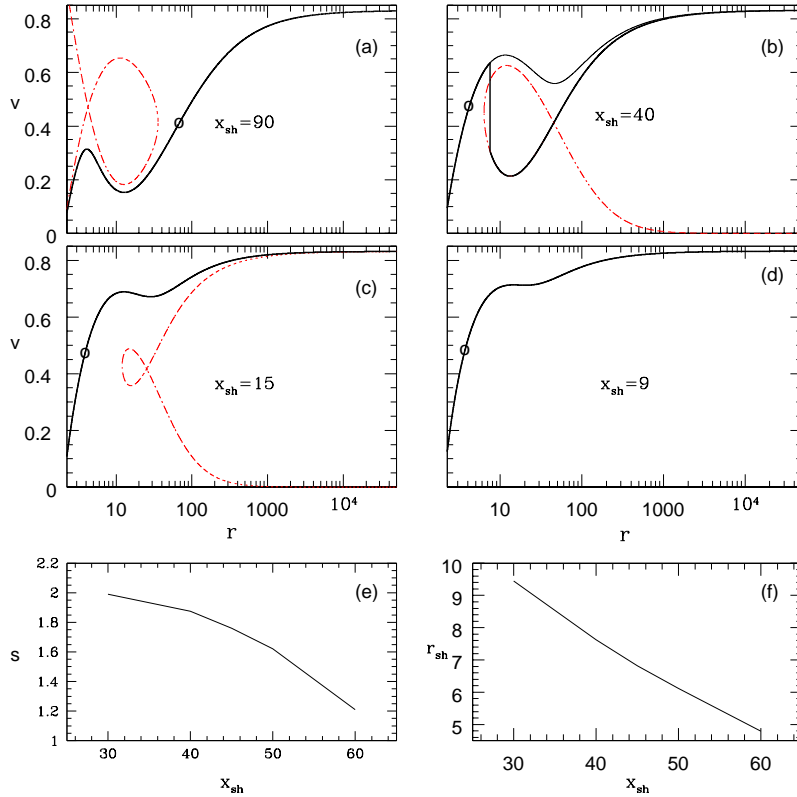


Figure 7. Variation of v along r for different values of x_{sh} as labeled in (a)-(d). The dotted (red) curves are closed solutions, while thin black solid curves are possible transonic solutions. Vertical line show stable shock transition (Thick solid). Thick solid curves are the realistic transonic solutions of the jet; (e) Shock strength S as a function of x_{sh} ; and (d) r_{sh} as a function of x_{sh} . Here $E = 1.8$, $\xi = 1.0$.

we show how the jet solution changes for different values of x_{sh} but keeping $E = 1.8$ of the jet same. For a large value of $x_{\text{sh}} = 90$ (Fig. 7a), the jet cross section near the base diverges so much that the jet loses the forward thrust in the subsonic regime and the sonic point is formed at large distance. The geometry indeed decelerates the flow, but being in the subsonic regime such deceleration do not accumulate enough pressure to break the kinetic energy and therefore no shock is formed. As the expansion of the cross-section is arrested, the jet starts to accelerate and eventually becomes transonic at large distance from the BH. At relatively smaller value of x_{sh} ($= 40$), the thermal term remains strong enough to negate gravity and form the sonic point in few r_g . For such values of x_{sh} , the fractional expansion of the jet cross-section drastically reduces or, $\mathcal{A}^{-1}d\mathcal{A}/dr \sim 0$, when the jet is supersonic. Therefore, in this case the jet suffers shock (Fig. 7b). Infact, for $E = 1.8$ the jet will under go shock transition, if the accretion disc shock location range is from $x_{\text{sh}} = 30$ – 60 . For even smaller value of accretion shock location $x_{\text{sh}} = 15$, because the opening angle of the jet is less, the thermal driving is comparatively more than the previous case. The jet becomes

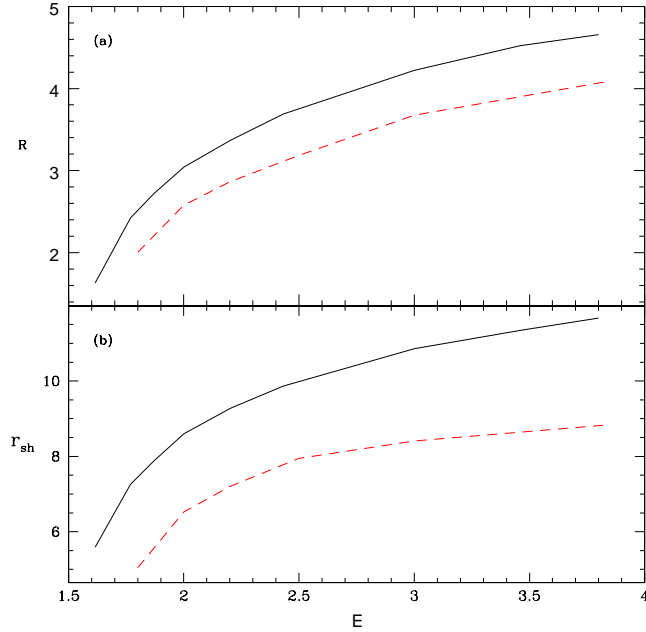


Figure 8. R (a) and r_{sh} (b) as functions of E for $x_{\text{sh}} = 40$ (solid) and $x_{\text{sh}} = 60$ (dashed, red)

supersonic at an even shorter distance. The outer sonic point is available, but because the shock condition is not satisfied, shock does not form in the jet (Fig. 7c). As the shock in accretion is decreased to $x_{\text{sh}} = 9$, the thermal driving is so strong that it forms only one sonic point, overcoming the influence of the geometry (Fig. 7d). Although, due to the fractional change in jet geometry, the nature of jet solutions have changed, but jets launched with same Bernoulli parameter achieves the same terminal speed independent of any jet geometry. This is because at $r \rightarrow \infty$, $h \rightarrow h_{\infty} \rightarrow 1 \Rightarrow u_t \rightarrow u_{t\infty} \rightarrow \gamma_{\infty}$, so

$$E = -hu_t = -h_{\infty}u_{t\infty} = \gamma_{\infty} = (1 - v_{\infty}^2)^{-1/2}.$$

or,

$$v_{\infty} = \left(1 - \frac{1}{E^2}\right)^{1/2}. \quad (33)$$

In Figs. (7e, f), the jet shock strength (equation 32) and the jet shock location r_{sh} are plotted as functions of accretion shock location x_{sh} .

In Figs. (8a, b), the shock compression ratio R (equation 31) of the jet and the jet shock location r_{sh} as a function of E is plotted. Each curve represents the accretion shock location $x_{\text{sh}} = 40$ (solid) and $x_{\text{sh}} = 60$ (dashed). It shows that for a given E , the jet shock r_{sh} and strength S decrease with the increase of x_{sh} . From Fig. (4a) it is also clear that for larger values of x_{sh} , jet shock may form in larger region of the parameter space. The compression ratio of the jet is above 3 in a large part of the parameter space, therefore shock

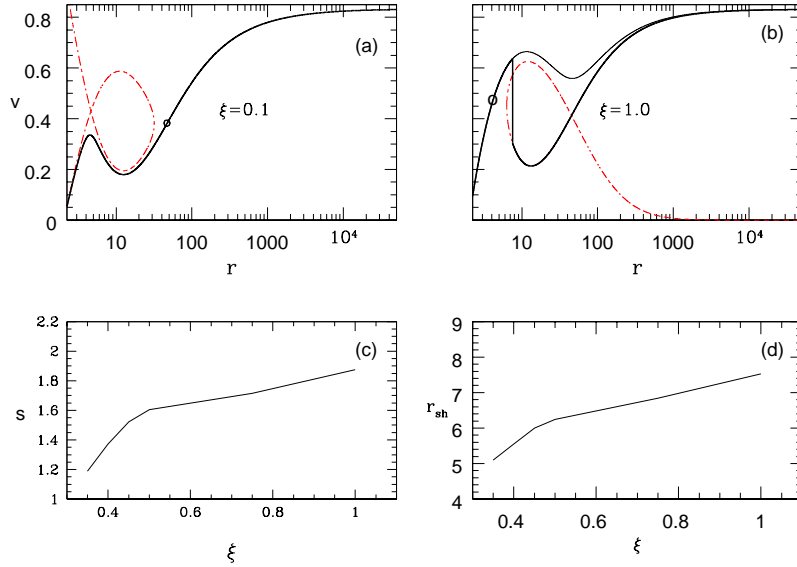


Figure 9. Variation of v with r for different values of $\xi = 0.1$ (a) and $\xi = 1.0$ (b), also labeled on the plots. Closed (dash) and global (solid) solutions. Thick solid (black online) curves show the transonic physical trajectory of the jet and the vertical line is the shock; (c) S and (d) r_{sh} with ξ plotted. For all panels $x_{\text{sh}} = 40$ and $E = 1.8$.

acceleration would be more efficient at these shocks. It is interesting to note the contrast in the behaviour of the jet shock r_{sh} with the accretion disc shock. In case of accretion discs, the shock strength and the compression ratio increases with decreasing shock location x_{sh} (Kumar & Chattopadhyay 2013; Chattopadhyay & Kumar 2016). But for the shock in jet, the dependence of R and S on r_{sh} is just the opposite i. e., R and S decreases with decreasing r_{sh} .

So far we have only studied the jet properties for $\xi = 1.0$ or, electron-proton ($e^- - p^+$) flow. In Newtonian flow, composition would not influence the outcome of the solution if cooling is not present. But for relativistic flow, composition enters into the expression of the enthalpy and therefore, even in absence of cooling, jet solutions depend on the composition. In Figs. (9a) we plot the velocity profile of a jet whose composition corresponds to $\xi = 0.1$ i. e., the proton number density is 10% of the electron number density, where the charge neutrality is restored by the presence of positrons. The jet energy is $E = 1.8$ and jet geometry is defined by $x_{\text{sh}} = 40$. In Fig. (9b), we plot the velocity profile of an $e^- - p^+$ jet ($\xi = 1.0$), for the same values of E and x_{sh} . While $e^- - p^+$ jet undergoes shock transition, but for the same parameters E and x_{sh} , for the flow with $\xi = 0.1$ composition, there is no shock. Infact, $\xi = 0.1$ jet solution is similar to the one with lower energy. Although, the jet solutions of different ξ are distinctly different at finite r , but the terminal speeds are same as is predicted by equation (33). For these values of E and x_{sh} , shock in jets are obtained for $\xi = 0.32 \rightarrow 1.0$.

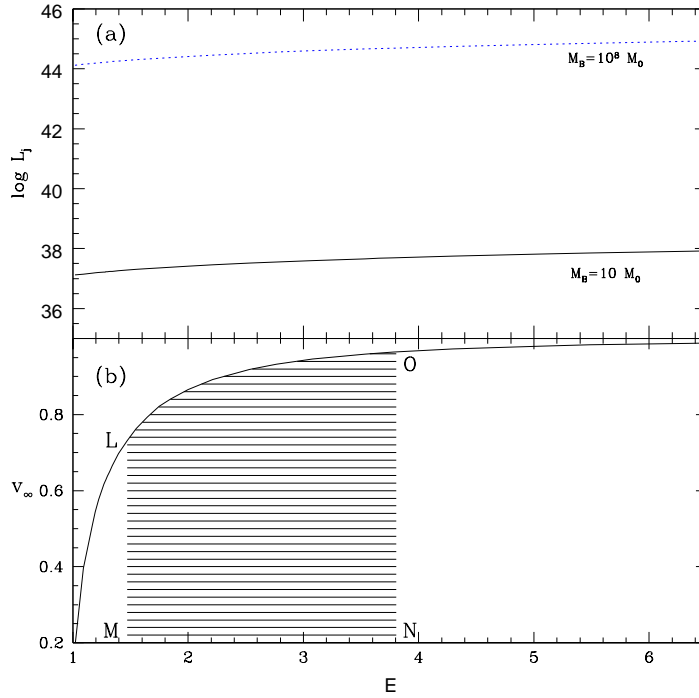


Figure 10. (a) v_∞ as a function of E . x_{sh} and ξ are kept 40 and 1.0 (b) $\log L_j$ with E for $M_B = 10^8 M_\odot$ (dot, blue) $M_B = 10 M_\odot$ (solid, black)

In Fig. (9c) and (9d) we plot shock strength S and the shock location r_{sh} respectively, as a function of ξ for the same values of E and x_{sh} . Shock produced in heavier jet ($e^- - p^+$) is stronger and the shock is located at larger distance from the BH. Figures (9c-d) again show that the shocks forming farther away from BH, are stronger.

Although AGN jets are directly observed and superluminal motions of bright spots directly observed, but still in most cases the jet speeds and jet kinetic power are generally inferred. However, few decades of continuous multi wavelength monitoring of the objects have lend reasonable credibility in the inferred values of L_j . From equations (21, 33), it is quite clear that in absence of dissipation both L_j and v_∞ are independent of jet geometry as well as, the composition of the flow. It must be remembered that, when expressed in terms of Eddington mass flow rate, L_j will depend on the central BH. In Fig. (10a), L_j is plotted as a function of E . The mass outflow rate is assumed to be $\dot{M}_{\text{out}} = 0.01 \dot{M}_{\text{Edd}}$. L_j scales with the mass of the BH and over a large range of E and for a central BH of mass $10^8 M_\odot$, L_j ranges from 10^{44-45} ergs s^{-1} (dotted), while for a $10 M_\odot$ BH, the kinetic power of the jet is 10^{37-38} ergs s^{-1} . These estimate would go up or down depending on the accretion rate, as well as the mass of the compact object. In Fig. (10b), v_∞ is plotted as a function of E . From equation (33) it is clear that v_∞ is a function of E only, except, when there are other

accelerating mechanism acting on the jet. So v_∞ in this figure is true for both M1 and M2 jets. However, if we assume $x_{\text{sh}} = 40$ for M2 jet and $\xi = 1.0$, then the shaded region LMNOL corresponds to jets which undergo steady shock transitions.

It might be fruitful to explore, whether these internal shocks satisfies some observational features. One may recall that the charged particles oscillates back and forth across a shock with horizontal width L and in each cycle, its energy keeps increasing. After successive oscillations, the particle escapes the shock region with enhanced energy known as e-folding energy and is given by (Blandford & Eichler 1987)

$$E_T = \frac{L(v_+ - v_-)B_{\text{sh}}}{\pi c} \left(\frac{\text{erg}}{\text{statC}} \right), \quad (34)$$

where B_{sh} is the magnetic field at the shock and $L = 2GM_B r_{\text{sh}} \tan \theta / c^2$. The typical magnetic field estimates near the horizon vary from $10mG$ (Laurent *et al.* 2011) to 10^4G (Kogan & Lovelace 1997). For $M_B \sim 14M_\odot$ (Cygnus X-1), the e-folding energy for the shock obtained in Fig. 7b is obtained to be $16MeV$ - $1.6TeV$ (per electron charge in statC) depending on different magnetic field estimates mentioned above. The energy associated with high energy tail of $400keV - 2MeV$ in Cygnus X-1 (Laurent *et al.* 2011) can easily be explained by the internal jet shocks discussed in this paper. The spectral index of shock accelerated particles is

$$q = \frac{R}{R - 1} \quad (35)$$

And for the same set of jet parameters we obtained $R = 1.87$ or $q = 2.15$, therefore, even the estimated spectral index of 2.2 ± 0.4 of such observational estimates (Laurent *et al.* 2011) can be given a theoretical basis.

5 DISCUSSION AND CONCLUDING REMARKS

In this paper, we investigated the possibility of finding steady shocks in jets very close to the compact object. Since the jets exhibit mildly relativistic to ultra relativistic terminal speeds, therefore, one has to describe the flow in the relativistic regime. The jets traverse massive length scales originating very close to the central BH to distances more than hundred thousand Schwarzschild radii, therefore gravitational effects need to be considered. And since relativity and any form of Newtonian gravity is incompatible, therefore, the jet has to be described as fluid flow in the general relativistic limit. In the present paper, we investigated jets in Schwarzschild metric and have used a relativistic equation of state (as opposed to

the Newtonian polytropic one) to describe the thermodynamics of the jet. Since jets are collimated and flows about the axis of symmetry, and as pointed out in section 2, the jet is generated with low angular momentum and it is likely to be further reduced by other physical processes like viscosity, we consider non rotating jets as an approximation.

In this paper we have studied two jet models. The first model M1 was the conical jet or radial outflow and the flow geometry is that of a cone. The second model M2 was assumed from physical argument and some evidence found in previous jet simulations. Since the jet base is supposed to be very hot therefore, it is expected that the jet would expand in all directions, only to be mechanically held by the funnel shaped inner surface of the torus-like inner disc. The expansion of the jet cross-section gets arrested above the inner torus like corona and then expands again at larger distances from the BH. We assumed a jet flow geometry which follows this pattern. It should also be remembered that, in this paper the accretion disc plays an auxiliary role. We did not compute any jet parameters from the accretion disc. We just used an approximate accretion disc solution to define the flow geometry at the base of the jet, and then used the outer boundary of the inner disc, or, x_{sh} as a parameter which defines the departure of the jet geometry from the conical cross-section. And to do that, we fitted the temperature distribution of the PSD by an approximated function, which would determine the inner surface of the torus part of the inner disc or PSD. That inner surface was considered as the outer boundary of the jet geometry close to the BH. The accretion disc solution used is exactly same as our previous paper Vyas *et al.* (2015), although unlike the previous paper, no other input from the accretion disc was used in the jet solution. One must remember that accretion solutions change for different values of disc parameters, although, in this paper the disc solutions do not influence jet solutions.

Since we have ignored other external accelerating mechanism or any dissipation, so E is a constant of motion. An adiabatic jet is a fair assumption until and unless the jet interacts with the ambient medium. Given these assumptions, terminal speed (v_{∞}) of the jet is solely governed by E and would not depend on either the jet geometry, or, the composition of the flow. However, the jet geometry influences the solutions at finite r from the BH. While M1 model showed monotonic smooth solutions, whose terminal speed increased with the increasing E . But for M2 model, depending on the jet energy E and the accretion disc parameter x_{sh} , we obtained very fast, smooth jets flowing out through one inner X-type sonic point; and for other combinations of E & x_{sh} , we obtained jets with multiple sonic points and even shocks. For very low E of course, weak jets flow out though the outer X-type sonic point.

In connection to Fig. 6 in section 4.2, it has been clearly explained that, in order to obtain steady state internal shocks, the jet material in the supersonic regime has to oppose the flow following it. That can happen if the expansion of the flow geometry drastically decrease when the jet is in the supersonic regime, making gravity relatively stronger. The effect would not be so effective at distances where gravity is itself weak. Therefore the necessary condition is that, the expansion of the jet geometry decreases drastically in few to $\text{few} \times 10r_g$. Along with this, E has to be high enough, so that the enhanced thermal driving makes the flow supersonic before the region where $\mathcal{A}^{-1}d\mathcal{A}/dr \sim 0$. One of the advantages of a shock driven by the jet geometry is that, it has no impact on either the kinetic power of the jet or, its terminal speed. So if E is high enough produce very strong jet with relativistic terminal speed, then in addition one may have shock jump in the jet without compromising the v_∞ . It should be understood, that in presence of other accelerating mechanism, E will not remain constant and would increase outwards. Therefore, the terminal speeds obtained here may be considered as the minimum that can be achieved for the given input parameters. The jet kinetic power (equation 21) obtained also depends on \dot{M} and E , so output would depend on the central mass and the mass supply. In our estimation of L_j we assumed higher mass outflow rate at the base, but general relativistic estimates of such mass loss is around few percent of the accretion rate, which can easily explain the estimates for Cygnus X-1 jet (Russel et. al. 2007)

Interestingly, for low values of x_{sh} , the jet geometry of M2 differs slightly from the conical one. Therefore, the jet shock is obtained in a very small range of E . For higher x_{sh} , the range of E which can harbour jet shocks also increases. However, at same E , the jet shock r_{sh} is formed at larger distance from the BH, if x_{sh} is formed closer to the BH. This is very interesting, because in accretion disc as the shock moves closer to the BH, the shock becomes stronger. In addition, smaller value of x_{sh} implies higher values of r_{sh} and higher r_{sh} means stronger jet shock. That means a very hot gas may surround the BH, not only in the equatorial plane but also around the axis as well. For the current objectives the detailed spectral analysis is beyond the scope of the paper and has not been done for such a scenario as yet, we would like to do that in future.

The assumptions made in this paper, were to simplify the jet problem and study all possible relativistic jet solutions possible in the presence of strong gravity. However, few things definitely would influence the conclusions of this paper positively. Consideration of radiation driving for intense radiation field would surely affect the jet solution. It would

surely accelerate the jets (see, Vyas *et al.* 2015), but in addition radiation drag in presence of an intense and isotropic radiation field may drive shocks, which means even M1 jet may harbour shocks. Moreover, the jet geometry need not be conical at large distances, and the jet geometry may be pinched off by other mechanisms, which might create more shocks. Furthermore, entrainment of the jet at large distances might qualitatively modify the conclusions of this paper. Even then, the result of this paper might be important in many other ways. From Figs. (6, 7, 8) it is clear that, farther the shock forms, stronger is the shock. Since the base of the jet is much hotter than even the post-shocked region, then any surge in mass outflow rate, or, energy/momentum enhancement in the base will try to drive the jet away from its stable position. If this driving is too strong, it will render the shock unstable and the shock would travel out along the jet beam. This should have two effects, the unshocked jet material will be shock heated, moreover, since by the nature of jet shocks, it becomes stronger for larger r_{sh} , therefore a shock traveling out would shock-accelerate jet particles quite significantly. And this would happen comparatively close to the jet base. However, if the driving is not too strong, this might lead to quasi periodic oscillations. Such shock oscillation model has not been properly probed even in micro-quasar scenario. This might even be interesting for QPOs in blazars. It must be remembered that, previously, we did not obtain standing internal shocks in jets around non-rotating BHs (Kumar & Chattopadhyay 2013, 2014; Chattopadhyay & Kumar 2016) for geometries assumed. The main aim of this paper is to show that, if jet geometries with non-spherical geometry is considered, then internal shocks may form close to the jet base and such solutions may address few observational features as well. And the assumptions made in this paper was aimed at reducing the frills, which might obfuscate the real driver of such shocks in jets.

Drawing concrete conclusions, one may say, M2 jets with energies $E = 1.5\text{--}2.5 c^2$ may harbour shocks in the range $r_{\text{sh}} = 5.5\text{--}10r_{\text{g}}$ from the central BH. The shocks are in the range of compression ratio $R = 1.6\text{--}4.0$. The terminal speeds of these jets are between $v_{\infty} = 0.745\text{--}0.916c$.

ACKNOWLEDGMENT

The authors acknowledge the anonymous referee for helpful suggestions to improve the quality of this paper.

REFERENCES

- Aharonian F. et al., 2007, *ApJ*, 664, L71.
- Beskin V. S., 2003, *Accretion Disks, Jets and High-Energy Phenomena in Astrophysics: Les Houches Session LXXVIII*, Springer Science and Business Media, p. 200-202
- Baade W., Minkowski R., 1954, *ApJ*, 119, 215
- Bisnovatyi-Kogan G. S., Lovelace R., 1997, *ApJ*, 486, L43
- Blandford R. and Eichler D., 1987, *Physics Reports*, 154(1), 1-75.
- Blumenthal G. R., Mathews W. G., 1976, 203, 714
- Biretta J. A., 1993, in Burgerella D., Livio M., Oea C., eds, *Space Telesc. Sci. Symp. Ser.*, Vol. 6, *Astrophysical Jets*. Cambridge Univ. Press, Cambridge, p. 263
- Biretta J. A., Sparks W. B., Macchetto F., 1999, *ApJ*, 520, 621
- Chakrabarti S.K., *ApJ*, 1989, 347, 365
- Chakrabarti S. K., Jin L., Arnett D., 1987, *ApJ*, 313, 674.
- Chakrabarti S. K., Titarchuk L., 1995, *ApJ*, 455, 623.
- Chattopadhyay I., Chakrabarti S. K., 2002a, *MNRAS*, 333, 454.
- Chattopadhyay I., Chakrabarti S. K., 2002b, *BASI*, 30, 313
- Chattopadhyay I., Das S., Chakrabarti S. K., 2004, *MNRAS*, 348, 846.
- Chattopadhyay I., 2005, *MNRAS*, 356, 145.
- Chattopadhyay I., Das S., 2007, *New A*, 12, 454.
- Chattopadhyay, I., 2008, in Chakrabarti S. K., Majumdar A. S., eds, *AIP Conf. Ser. Vol. 1053, Proc. 2nd Kolkata Conf. on Observational Evidence of Black Holes in the Universe and the Satellite Meeting on Black Holes Neutron Stars and Gamma-Ray Bursts*. Am. Inst. Phys., New York, p. 353
- Chattopadhyay I., Chakrabarti S.K., 2011, *Int. Journ. Mod. Phys. D*, 20, 1597.
- Chattopadhyay I., Kumar, R., 2016, *MNRAS*, 459, 3792.
- Chattopadhyay I., Ryu D., 2009, *ApJ*, 694, 492
- Chattopadhyay I., Ryu D., Jang, H., 2013, *AsInc*, 9, 13.
- Das S., Chattopadhyay I., Nandi A., Molteni D., 2014, 442, 251.
- Doeleman S. S. et al., 2012, *Science*, 338, 355.
- Dove J. B., Wilms J., Maisack M., Begelman M. C., 1997, *ApJ*, 487, 759
- Falcke H., 1996, *ApJ*, 464, L67
- Fender R. P., Belloni T. M., Gallo E., 2004, *MNRAS*, 355, 1105

- Fender R. P., Gallo E., Russell D., 2010, MNRAS, 406, 1425.
- Ferrari A., Trussoni E., Rosner R., Tsinganos K., 1985, ApJ, 294, 397.
- Fukue J., 1987a, PASJ, 39, 309
- Fukue J., 1987b, PASJ, 39, 679
- Fukue J., 1996, PASJ, 48, 631
- Fukue J., 2000, PASJ, 52, 613
- Fukue J., Tojyo M., Hirai Y., 2001, PASJ 53 555
- Gallo E., Fender R. P., Pooley G. G., 2003 MNRAS, 344, 60
- Gierlinski et. al., 1997, MNRAS, 288, 958
- Hu T., Peng Q., 2008, ApJ, 681, 96103
- Junor W., Biretta J.A., Livio M., 1999, Nature, 401, 891
- Kataoka J., et. al., 2001, ApJ, 560, 659
- Kopp R. A., Holzer T. E., 1976, Solar Phys., 49, 43
- Kudoh T., Matsumoto R., Shibata K., 2002, PASJ, 54, 121
- Kumar R., Chattopadhyay I., 2013, MNRAS, 430, 386.
- Kumar R., Singh C. B., Chattopadhyay I., Chakrabarti S. K., 2013, MNRAS, 436, 2864.
- Kumar R., Chattopadhyay I., Mandal, S., 2014, MNRAS, 437, 2992.
- Kumar R., Chattopadhyay I., 2014, MNRAS, 443, 3444.
- Laing R. A., Bridle A. H., 2002, MNRAS, 336, 328
- Laurent P., Rodriguez J., Wilms J., Bel M. C., Pottschmidt K., Grinberg V., 2011, Science 332.6028, 438-439
- Liang E. P. T., Thompson K. A., 1980, ApJ, 240, 271L
- Lee S.-J., Chattopadhyay I., Kumar R., Hyung S., Ryu D., 2016, ApJ, 831, 33
- Maitra D., Miller M. J., Markoff S., King A., 2011, ApJ, 735, 107
- Margon B., 1984, ARA&A, 22, 507
- Marti J., Muller E., Font J. A., Ibanez, J. M., Marquina, A., 1997, ApJ, 479, 151.
- McHardy I. M., Koerding E., Knigge C., Fender R. P., 2006, Nature, 444, 730
- Memola E., Fendt C. H., Brinkmann W., 2002, A&A 385, 1089
- Michel F. C., 1972, Ap&SS, 15, 153
- Miller-Jones J. C. A., Sivakoff G. R., Altamirano D., et al. 2012, MNRAS, 421, 468
- Mirabel I. F., Rodriguez L. F., Cordier B., Paul J., Lebrun F., 1992, Nature, 358, 215
- Mirabel I. F., Rodriguez L. F., 1994, Nature, 371, 46
- Moellenbrock G. A., Fujisawa K., Preston R. A., Gurvits L. I., Dewey R. J., Hirabayashi

- H., Jauncey D. L., 1996, AJ, 111, 2174
- Narayan R., Kato S., Honma F., 1997, ApJ, 476, 49
- Novikov I. D., Thorne K. S., 1973, in Dewitt B. S., Dewitt C., eds, Black Holes. Gordon and Breach, New York, p. 343
- Nakayama K., 1996, MNRAS, 281, 226
- Paczyński B. and Wiita P.J., 1980, A&A, 88, 23
- Perlman E. S., Wilson A. S., 2005, ApJ, 627, 140
- Rushton A., Spencer R., Fender R., Pooley G., 2010, A&A, 524, 29.
- Russell D. M., Fender R. P., Gallo E., Kaiser C. R., 2007, MNRAS, 376, 1341
- Ryu D., Chattopadhyay I., Choi E., 2006, ApJS, 166, 410.
- Sikora M., Wilson D. B., 1981, MNRAS, 197, 529.
- Shakura N. I., Sunyaev R. A., 1973, A&A, 24, 337S.
- Taub A. H., 1948, Phys. Rev., 74, 328
- Vlahakis N., Tsinganos K., 1999, MNRAS, 307, 279
- Vyas M. K., Kumar R., Mandal S., Chattopadhyay I., 2015, MNRAS, 453, 2992.
- Wardle J. F. C., Aaron S. E., 1997, MNRAS, 286, 425
- Yang R., Kafatos M., 1995, A&A, 295, 238
- Yuan F., Dong S., Lu J.-F., 1996, Ap&SS, 246, 197
- Zensus J. A., Cohen M. H., Unwin S. C., 1995, ApJ, 443, 35

APPENDIX A: STABILITY ANALYSIS OF THE SHOCKS

In section 4, we reported existence of 2 shocks, present at either sides of middle sonic point in various solutions. One of the two such shocks were shown to be unstable previously (Nakayama 1996; Yang & Kafatos 1995; Yuan et. al. 1996). We include the stability analysis for the sake of completeness. The momentum flux, T^{rr} (equation 28), remains conserved across the shock. But if the shock under some perturbation, moves from r_{sh} to $r_{\text{sh}} + \delta r$ then T^{rr} may not be balanced. The resultant difference across the shock is

$$\delta T^{rr} = T_2^{rr} - T_1^{rr} = \left[\left(\frac{dT^{rr}}{dr} \right)_2 - \left(\frac{dT^{rr}}{dr} \right)_1 \right] \delta r = \Delta \delta r \quad (\text{A1})$$

Multiplying and dividing equation (28) by ρ and after rearranging the expression for momentum flux becomes

$$T^{rr} = \rho \left(hu^r u^r + \frac{2\Theta g^{rr}}{\tau} \right) \quad (\text{A2})$$

Now using equation (14) and differentiating equation (A2) followed by some algebra, one obtains

$$\frac{dT^{rr}}{dr} = \frac{\dot{M}_{out}}{\mathcal{A}\tau} \left[-A_s \frac{dv}{dr} + B_s \right], \quad (\text{A3})$$

where,

$$A_s = \sqrt{g^{rr}} \gamma^3 \left[\frac{2\Theta g^{rr}}{u^2} + (f + 2\Theta) \right] + \frac{2\Theta \gamma^2}{Nuv} \left(u^2(N + 1) + g^{rr} \right) \quad (\text{A4})$$

and

$$B_s = \frac{\gamma v}{r^2 \sqrt{g^{rr}}} \left[(f + 2\Theta) - \frac{2\Theta g^{rr}}{u^2} \right] - \left((f + 2\Theta)u^2 + 2\Theta g^{rr} \right) \frac{1}{u\mathcal{A}} \frac{d\mathcal{A}}{dr} + \frac{4\Theta}{ur^2} - \frac{2\Theta}{Nu} \left[u^2(N + 1) + g^{rr} \right] \quad (\text{A5})$$

Using equation (A3) in (A1), we obtain

$$\Delta = [-A_s v' + B_s] = (A_{s1} v'_1 - A_{s2} v'_2) + (B_{s2} - B_{s1}) \quad (\text{A6})$$

Now, the stability of the shock depends on the sign of Δ . If $\Delta < 0$ for finite and small δr there is more momentum flux flowing out of the shock than the flux flowing in so the shock keeps shifting towards further increasing r , and is unstable. On the other hand if $\Delta > 0$, then the change due to δr leads to the further decrease in Δ , and the shock is stable.

One finds that equations (A4) and (A6) A_s has positive value. Now the stability of the shock can be analyzed under two broad conditions.

- Condition 1. The shock is significantly away from middle sonic point, or the absolute magnitude of v' is significantly more than 0. We find that $|B_s| \ll |A_s|$ and hence the stability of the shock depends upon the sign of v' . Equation (A1) shows that the shock is stable (or $\Delta > 0$) if $v'_1 > 0$ and subsequently $v'_2 < 0$. Hence the inner shock is stable and the outer shock is unstable.
- Condition 2. If the shock is close to the middle sonic point, $v'_1 \approx v'_2 \approx 0$. So only second term consisting B_s contributes to the stability analysis and one obtains that $\Delta < 0$ for both inner and outer shocks and the shock is always unstable.

Finally, the general rule for stability of the shock is,

- If the post shock flow is accelerated then the shock is unstable and if the post shock flow is decelerated the shock is stable unless the shock is very close to the middle sonic point where it is unstable.

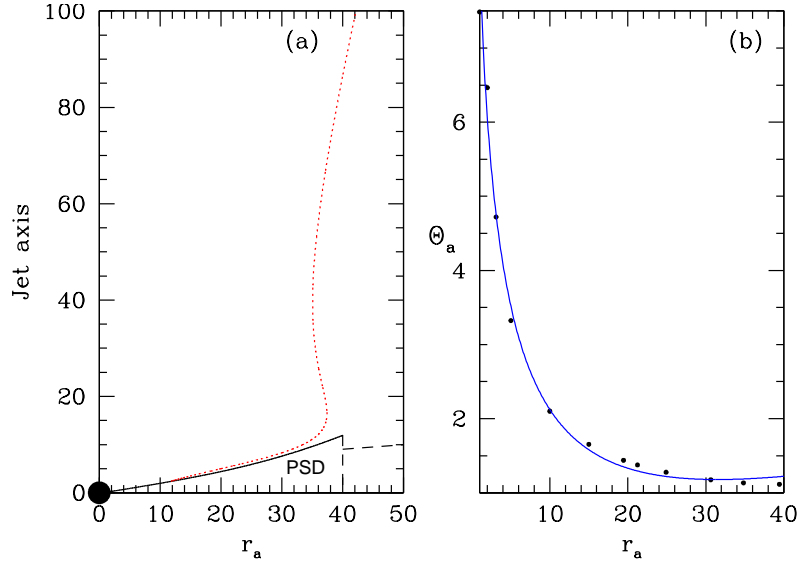


Figure B1. (a) Accretion disc height H_a is plotted with r_a with solid line (black online). Shock location is at $x_{sh} = r_a = 40$, shown by long dashed line. The jet width $r \sin \theta$ is over plotted with red dotted line. Black hole resides at $r_a = 0$ with shown as black sphere with $r_s = 2$ (b) Fitted Θ_a .

In the paper all the stable shocks are shown by thick solid vertical lines and unstable shocks are represented by thin dotted vertical lines.

APPENDIX B: APPROXIMATED ACCRETION DISC QUANTITIES

The jet geometry of M2 model was taken according to equation (4). The inner part of the accretion disc or PSD shapes the jet geometry near the base. If the local density, four velocity, pressure and dimensionless temperature in the accretion disc are p_a , u_a^r , ρ_a and Θ_a , respectively, and the angular momentum of the disc is λ , then the local height H_a of the post shock region for a advective disc is given by (Chattopadhyay & Chakrabarti 2011)

$$H_a = \sqrt{\frac{p_a}{\rho_a} [r_a^3 - \lambda^2(r_a - 2)]} = \sqrt{\frac{2\Theta_a}{\tau} [r_a^3 - \lambda^2(r_a - 2)]}, \quad (\text{B1})$$

where, r_a is the equatorial distance from the black hole. We obtain Θ_a in an approximate way following Vyas *et al.* (2015). The u_a^r is obtained by solving geodesic equation. Since u_a^r is known at every r_a , and accretion rate is a constant, so ρ_a is known. We also know that Θ_a and ρ_a are related by the adiabatic relation. So supplying Θ_a , ρ_a and u_a^r at the x_{sh} , we know Θ_a for all values of r_a . We plot the Θ_a in Fig. (B1b) for $x_{sh} = 40$ in filled dots. We obtain an analytic function to the variation of Θ_a with r_a . The obtained best fit is

$$\Theta_a = \exp(-r_a^{a_t} + b_t)c_t + d_t r. \quad (\text{B2})$$

Here, $a_t = 0.391623$, $b_t = 2.30554$, $c_t = 2.22486$ and $d_t = 0.0225265$. This fit is shown in

Fig. (B1-b) by solid line with points being actual values of Θ_a . The fitted function is used to compute H_a and is plotted in Fig. (B1-a) with solid line. We over plot the jet structure (equation 4) in red dots.